ELSEVIER

Ceramics International 31 (2005) 1109–1115

CERAMICS INTERNATIONAL

www.elsevier.com/locate/ceramint

Synthesis of nanophase tungsten carbide by electrical discharge machining

Ming-Hong Lin *

Department of Mechanical Engineering, National Kaohsiung University of Applied Sciences, Kaohsiung 80782, Taiwan, ROC

Received 12 October 2004; received in revised form 26 October 2004; accepted 2 December 2004
Available online 8 February 2005

Abstract

Tungsten carbide nanopowders were synthesized successfully by electric discharge machining followed by annealing under a nitrogen atmosphere. The tungsten workpieces were initially melted and evaporated on the working surface during the electric discharge machining process, and then the tungsten powders were reacted with the carbon electrode and the working medium of kerosene to form the nanocrystalline WC_{1-x} powders. The powders produced were characterized by XRD, SEM, and TEM. When annealing the powders under an N_2 atmosphere, the cubic phases of WC_{1-x} gradually changed to hexagonal W_2C and then were transformed fully to nanocrystalline hexagonal WC at 1200 °C, with the nanocrystalline tungsten carbide encapsulated in a carbon shell. On the other hand, under an H_2 atmosphere, the WC_{1-x} phase changed via a W_2C phase to reduced powders of pure tungsten at 1000 °C or were reduced directly from WC_{1-x} to elemental W.

Keywords: Tungsten carbide; Nano-powder; Electrical discharge machining

1. Introduction

Hexagonal tungsten carbide (WC) is an important tool and die material [1–4] mostly because of its high melting point (2800 °C), high degree of hardness (H_v = 22 GPa), high modulus of elasticity (696 GPa), high fracture toughness (28 MPa $m^{1/2}$), and good wear resistance over a wide range of temperatures [5]. WC is a refractory cermet that has good thermal and chemical stability and is highly desirable because of the combination of its hardness, good abrasion and oxidation resistance, a low coefficient of thermal expansion (5.2 μm/m/K) [5], and a certain amount of plasticity.

Research into nanosized powders (1–100 nm) has recently become an important field in materials science. Nanosized powders have special optical, electronic, thermal, chemical, and other physical properties—for example, surface reactivity [6,7]. Recent experiments [8,9] have shown that WC–Co composites of nanoparticles have superior mechanical properties because of their improved hardness and increased ductility and plasticity. The highly specific reactivities of the surface areas of nanoparticle WC have been applied in industrial catalysis as substitutes for noble metals, such as Pt, Pd, and Ir [8–13].

Conventionally, the process of manufacturing WC is performed by the direct reaction of carbon and tungsten at a high temperature (1400–1600 °C) [3]. Three methods are commonly used to obtain WC powders: (1) Mixtures of tungsten and carbon powders are sintered in the graphite tube of induction or electrical resistance furnaces under a hydrogen atmosphere; (2) tungsten oxides are reacted with carbon at high temperature; and (3) tungsten powders are heated under a methane atmosphere. The powder sizes of WC obtained using these methods are >150 nm [14].

The traditional chemical process for synthesizing nanoparticle WC powders is the reductive decomposition of a W-based precursor, followed by its reaction with carbon [15–24]. Mechanical manufacturing methods have also been used to mix tungsten powder with carbon black and then to grind them together in a high-energy ball miller [25–28]. Metallic tungsten and carbon powders have been

* Fax: +886 7 3831373.
E-mail address: mhlin@cc.kuas.edu.tw

0272-8842/$30.00
doi:10.1016/j.ceramint.2004.12.004

simultaneously crushed and reacted at lower temperatures to form fine WC powders. Cubic WC_{1-x} powders of ultra-fine size (12 nm) can be produced using an ion-arc method in which tungsten and graphite electrodes are reacted with one another [29], but the hexagonal WC phase was not found when using this method.

Electric discharge machining (EDM) is used to cut and remove material by arc erosion of all kinds of electro-conductive materials. During the EDM processing, the melted work-piece reacts with electrode and then is rapid solidified in dielectric liquid to form powder debris. The present study proposes an attractive technique for preparing nanocrystalline powders of cubic WC_{1-x} and hexagonal WC by electric discharge machining and annealing processes.

2. Experimental

The electric discharge machining of 10-mm diameter tungsten rods was performed in kerosene fluid using a graphite electrode and a discharging current of 15–20 A. The debris was corrected in the fluid, cleaned with acetone, dried at 100 °C, and then annealed at 800–1600 °C under N_2 or H_2 atmospheres. The microstructures were observed by scanning electron microscopy (SEM, JEOL JEM6400). X-Ray diffraction (XRD, Siemens D5000; Cu Kα radiation) and transmission electron microscopy (TEM, JEOL AEM 3010; operated at 300 kV) were used to identify the phase changes before and after annealing for the debris powders. The powders for TEM analysis were prepared by mixing small amounts of ethanol (2 mL) and stirring for 1 min. Two or three drops of the suspension were placed on a Cu microgrid and then dried well for ca. 5 min before mounting the microgrid onto the TEM sample holder. The average particle sizes of the powders were calculated by the Scherrer formula using the XRD line broadening method [30]:

$$t = \frac{0.9\lambda}{B\cos\theta}$$

where t = the diameter of the crystal particle, λ = the wavelength of the X-ray radiation, B = the full width at half maximum height, and θ = the diffraction angle.

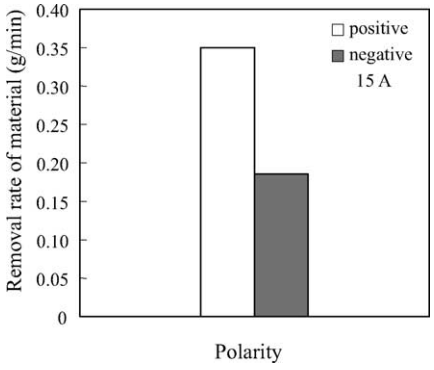

Fig. 1. The relationship between the removal rate of materials and the polarity.

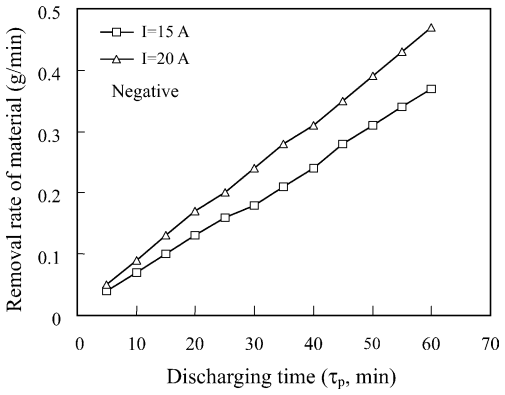

Fig. 2. The relationship between the removal rate of materials and the discharging time (τ_p, min).

3. Results and discussions

3.1. The effects of polarity and discharging current on removal rate of material

The high temperatures (8000–12,000 °C) used during discharging at the local region causes the work-pieces and

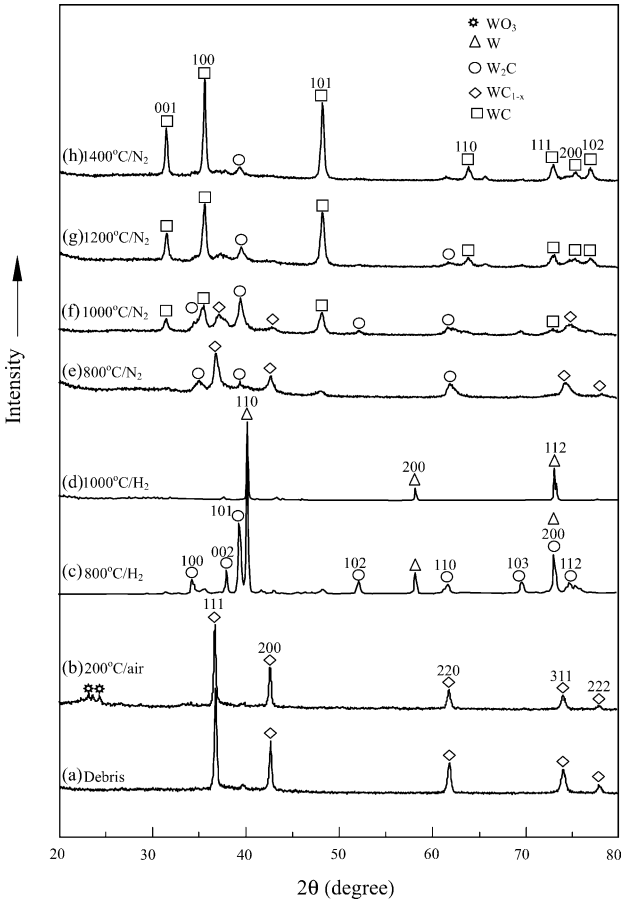

Fig. 3. XRD reflections of the particles (a) of debris, and the particles that were annealed at (b) 200 °C in air, (c) 800 °C under H_2, (d) 1000 °C under H_2, (e) 800 °C under N_2, (f) 1000 °C under N_2, (g) 1200 °C under N_2, and (h) 1400 °C under N_2.

electrodes to melt and evaporate. The dielectric fluid expands and applies high pressure (40–50 kg/cm^2) to the melting metal and electrode, which become atomized to create fine particles. The debris is produced as atomized fine particles react with the surrounding atmosphere and condense. In this study, the melted tungsten on the electric-discharged electrodes in kerosene reacted with the graphite electrode and carbon arising from the decomposition of kerosene to form the WC particles. The quantity of WC particles produced depends on the removal rate of the material, and other factors, such as the polarity-discharging current, the discharging time (τ_p), and the time of the discharging intermission (τ_t), that are related to the removal rate of the material. Fig. 1 provides a comparison of the removal rates of material between positive and negative electrodes (15 A) over a discharging time of 30 min, and indicates that the removal rate of material is higher for positive electrodes, because of the flow of electrons and ions [31].

In this study, graphite electrodes of negative polarity were used to obtained WC powders. Fig. 2 displays that the removal rates of tungsten at a discharging current of 20 A are higher than at 15 A. The removal rates of tungsten are proportional to the discharging time; we measured that 22 and 28 g of tungsten were removed at discharging currents of 15 and 20 A, respectively, during a discharging time of 60 min. The phases and particle sizes examined by XRD are similar for the debris particles obtained at either of these discharging currents.

3.2. XRD pattern of powders

The debris obtained from electric-discharge machining with 10–20 A discharging currents, followed by drying at 100 °C, were examined by XRD. Fig. 3a presents the same phases as those of fcc WC_{1-x} (JCPDS 20-1316) with a lattice constant of 0.042 nm. The WC_{1-x} phase is an interstitial solution of carbon in a fcc tungsten matrix. This

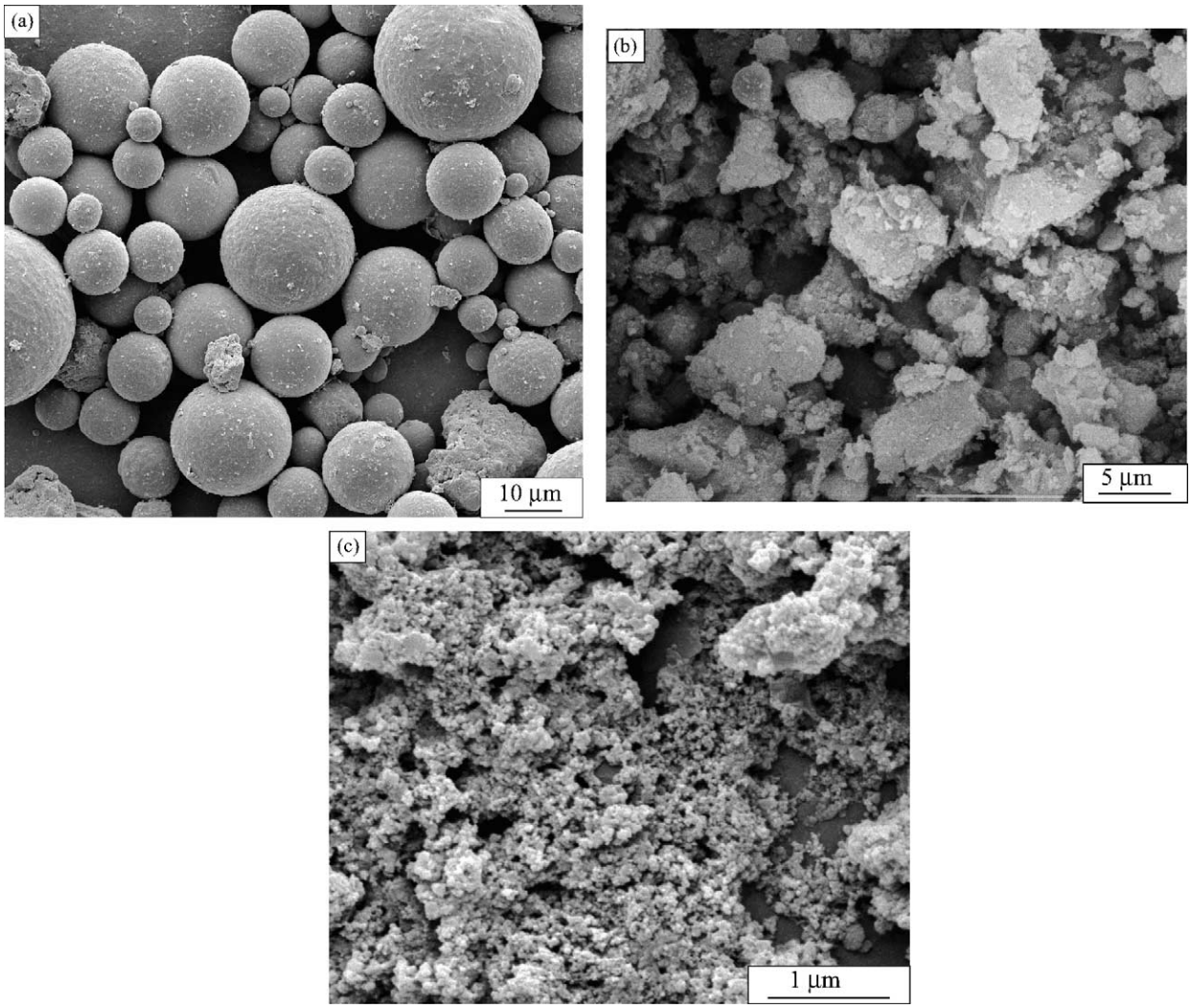

Fig. 4. SEM morphologies for powders (a) of debris, (b) after grinding, and (c) after annealing at 1400 °C under an N_2 atmosphere.

phase is similar to the WC compound obtained from the arc method [29] and from some of the rapid cooling experiments, such as splat quenching during thermal spraying or thin-film deposition during laser cladding [32–35]. The WC_{1-x} phase is stable above 2525 °C, but may not be stable at ambient temperature after slowly cooling [36]. The WC_{1-x} phase reacted with oxygen when the debris particles were dried at temperatures >100 °C. The XRD pattern in Fig. 3b reveals that the debris of the WC_{1-x} phases easily form oxides, such as WO_3, when drying at a temperature of 200 °C in air. This oxidation could be avoided by using H_2 or N_2 atmospheres.

3.2.1. Annealing under H_2

The XRD patterns in Fig. 3c and d present the phases of the debris annealed under an H_2 atmosphere and indicate that such annealing causes carbon depletion by the reaction of hydrocarbons and that the reduction of the WC_{1-x} phases induces the formation of di-tungsten carbide (W_2C) and tungsten (W) at 800 °C. When the temperature was increased to 1000 °C, W_2C also may reduce to elemental W, as indicated in Fig. 3d.

3.2.2. Annealing under N_2

The WC_{1-x} debris was annealed at 800–1400 °C under an N_2 atmosphere; Fig. 3e indicates that the carbon may not react and be exhausted when heating this way. From the phase diagram of W and C [36] below 2520 °C, the stable phases are W_2C and WC, but other WC_{1-x} species may occur with rapid cooling. The metastable phase of WC first forms when annealing at 800 °C, as indicated in Fig. 3e. The large amount of WC may be produced as the temperature rises up to 1000 °C. When heating to 1200 and 1400 °C, mostly stable WC phases occurs and these results agree well with carbon-rich region in the phase diagram. Therefore, the reaction paths of the high-temperature phases of WC are proposed as follows:

$$WC_{1-x} \rightarrow W_2C \rightarrow WC \rightarrow W_2C \rightarrow WC \quad (1)$$

3.3. SEM morphology of powders

The debris of the powders produced by electric discharge machining has spherical morphology (Fig. 4a). From Fig. 3a, we know that the XRD phase analysis confirms that the major phase is WC_{1-x}. Each agglomerated particle has a diameter of 5–30 μm. The powder debris consists of several million particles of fine WC_{1-x} and a small amount of graphite and retained hydrocarbon compounds; all of these species are connected to one another. The SEM micrograph in Fig. 4b displays the debris of the powder that was crushed to break the spherical agglomerates. The large particle agglomerates have sizes in the range 3–10 μm; irregular morphologies dominate the structure of the powder debris. The debris of powders had agglomerates that could be separated readily, however, through a subsequent annealing.

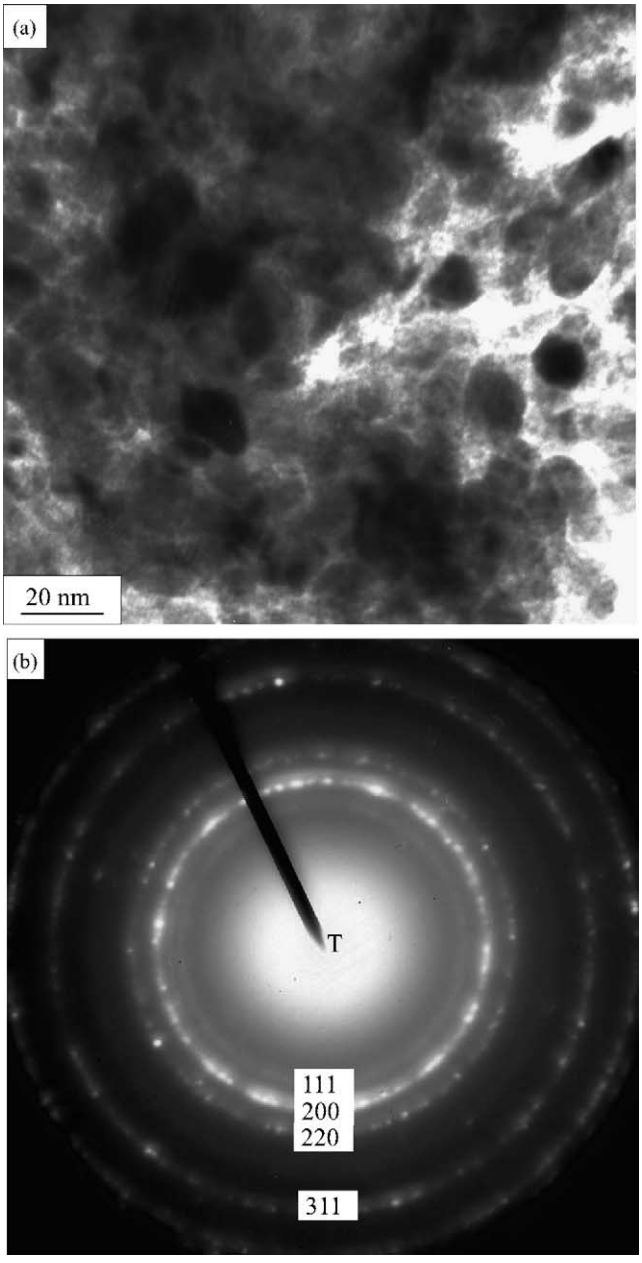

Fig. 5. TEM results for debris powders: (a) bright-field image; (b) diffraction patterns.

Fig. 4c displays the loosely agglomerated nanosized WC particles with rounded morphologies that occur upon removal of the retained hydrocarbon compounds during the transformation of the WC_{1-x} crystalline structure to the WC phase at 1400 °C under an N_2 atmosphere (cf. Fig. 3h).

3.4. TEM observations

Fig. 5a and b present a bright-field TEM image and a selected area diffraction pattern (SADP), respectively, for the powder debris; cubic WC_{1-x} agglomerates having rounded shapes and 10–20 nm sizes are observed. The selected area diffraction ring patterns clearly demonstrate

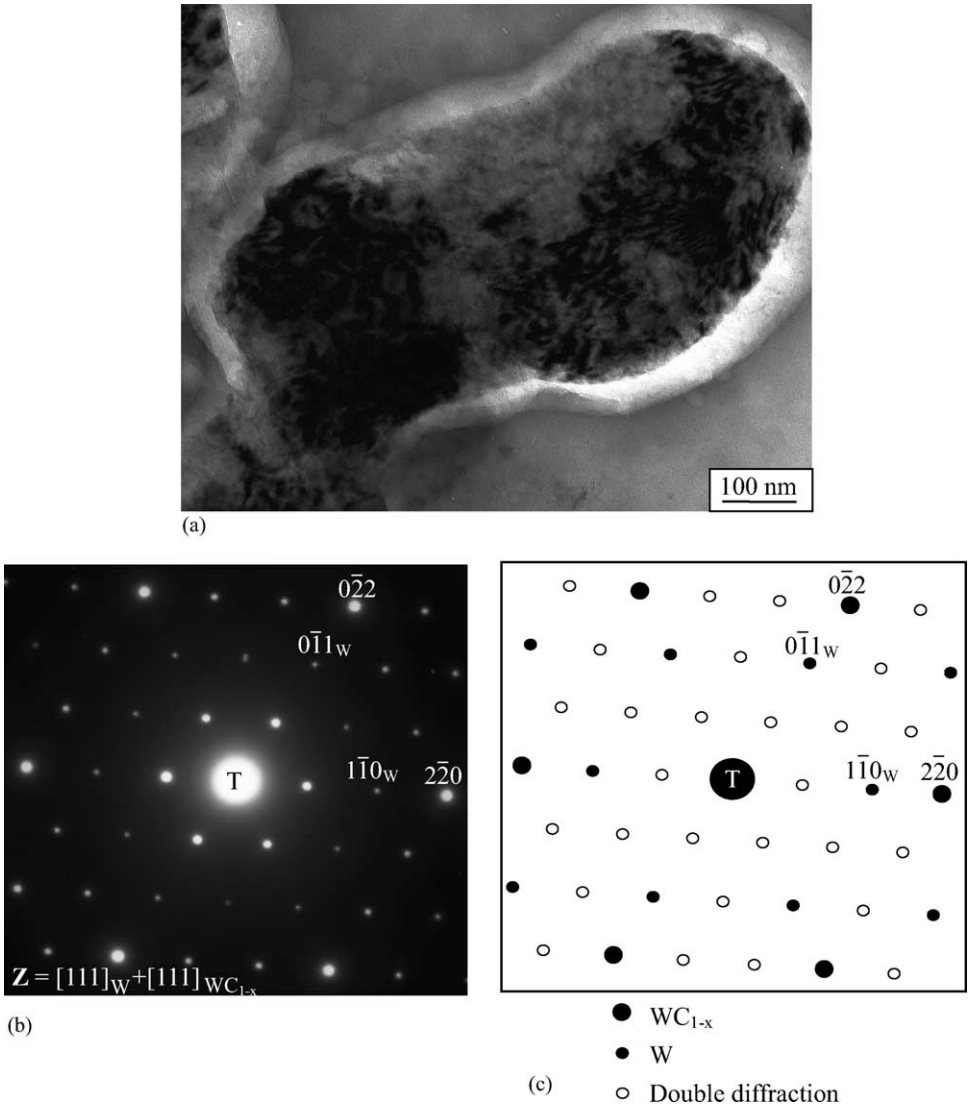

Fig. 6. TEM results for the particles annealed at 800 °C under an H_2 atmosphere: (a) bright-field image of nanophase cubic WC_{1-x}; (b) SADP; (c) a schematic diffraction pattern corresponding to the image in (b).

the nanocrystalline nature of the particles. The diffusive rings of the selected area diffraction pattern (Fig. 5b) suggest that the amorphous structures consist of retained hydrocarbon compounds.

Fig. 6a and b present the TEM bright-field image (BFI) and the SAPD, respectively, of the debris annealed 800 °C under an H_2 atmosphere. The BFI reveals a core-shell structure and the SADP arises from two phases, i.e., WC_{1-x} and W, and a double-diffraction effect. Fig. 6c presents an indexed illustration of the SADP; the smaller full circles represent the reflection planes of elemental W with zone axis $Z = [1\ 1\ 1]$, and the open circles are double-diffraction reflections. Therefore, the core-shell structure in Fig. 6a indicates the decarburized morphology of fcc WC_{1-x} powders as it becomes bcc elemental W. This phenomenon indicates that the diffusivity of carbon in tungsten is very high [37] and that the carbon atoms in tungsten diffuse very fast to the surface, which results in carbon depletion in the shell. TEM beams from WC_{1-x} powders coated with elemental W appear to cause the double-diffraction effect in the SADP [38]. According to this diffraction pattern (Fig. 6b), the orientational relationship between WC_{1-x} and W is $(1\ 1\ 0)_{WC_{1-x}}$ // $(1\ 1\ 0)_W$ and // $[1\ 1\ 1]_{WC_{1-x}}$ $[1\ 1\ 1]_W$, which occurs when fcc WC_{1-x} reduces to bcc elemental W. Combining these results with the XRD examinations (Fig. 3c and d), the two annealing reaction paths for the high-temperature phases of WC_{1-x} in an H_2 atmosphere are proposed in Eqs. (2) and (3).

$$WC_{1-x} \rightarrow W_2C \rightarrow W \quad (2)$$

$$WC_{1-x} \rightarrow W \quad (3)$$

Eq. (2) represents the first transformation to W_2C and then reduction to elemental W, and Eq. (3) reflects the direct reduction to elemental W.

The high-temperature phase of WC_{1-x} may become transformed to hexagonal WC when annealed at >1000 °C

Table 1
Average particle size of the WC nanopowders as calculated by the Scherrer formula

Temperature (°C)	Average particle size (nm)
1200	22
1400	29
1600	34

under an N_2 atmosphere, as deduced from the XRD results. Table 1 lists the average particle sizes for the WC powders as calculated by the Scherrer formula. As the temperature increases from 1200 to 1600 °C, the calculated average particle size increases from 22 to 34 nm. The sizes estimated from XRD are in good agreement with the sizes derived from transmission electron microscopy. Fig. 7a and b present the bright-field image and SADP, respectively, of the WC powders annealed at 1600 °C under a N_2 atmosphere; it appears that non-aggregated, rounded WC nanoparticles have formed. The sizes of the nanoparticles are 15–50 nm. The SADP in Fig. 7b, however, presents the weak reflection rings of the graphite powders; this image indicates that nanocrystalline tungsten carbide is encapsulated in a carbon shell, which is also the species that was found when using the ion arc method [29].

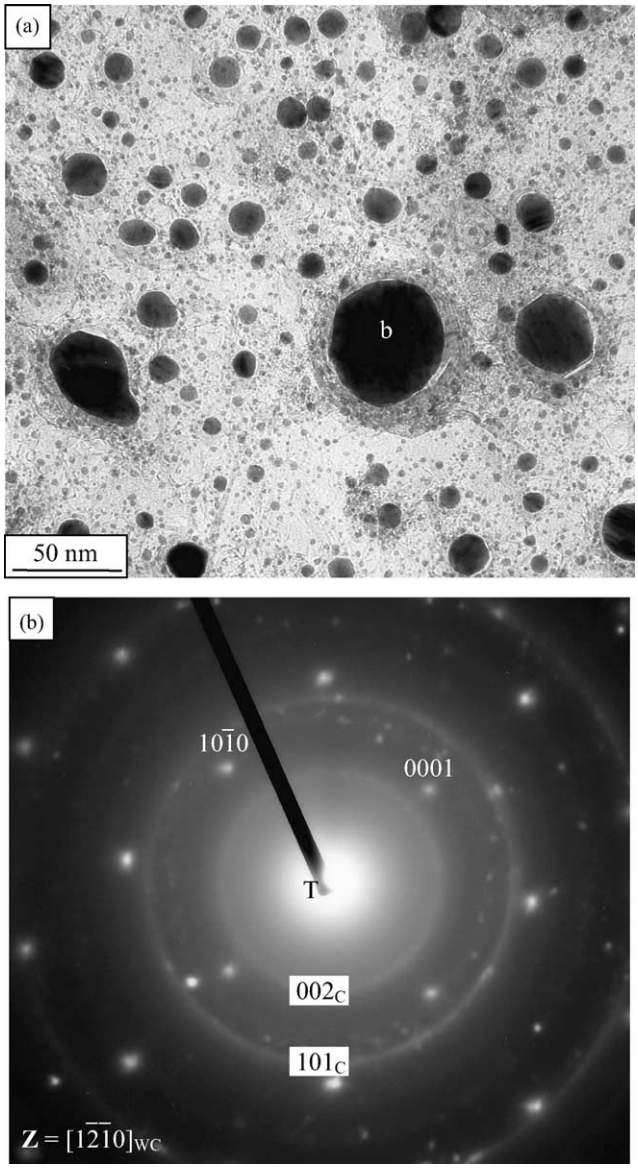

Fig. 7. TEM results for the particles annealed at 1600 °C under an N_2 atmosphere: (a) bright-field image of nanophase hexagonal WC; (b) the corresponding SADP of the particle labeled "b" in (a).

4. Conclusions

(1) The debris is a high-temperature-stable phase of WC_{1-x} that is oxidized readily when heating in air.
(2) WC_{1-x} is transformed to elemental W through two paths under an H_2 atmosphere. In one, WC_{1-x} is reduced directly to elemental W and, in the other, WC_{1-x} is first transformed to W_2C, which is then reduced to elemental W at 1000 °C.
(3) WC_{1-x} is first transformed to the hexagonal W_2C phase when annealed under an N_2 atmosphere, and then gradually it becomes nanoparticular hexagonal WC at 1200 °C. The nanocrystalline tungsten carbide is encapsulated in a carbon shell.

Acknowledgment

This research was funded by the National Science Council of Taiwan through NSC-91-2212-E-151-005.

References

[1] P. Schwartzkopf, R. Kieffer, Refractory Hard Metals—Borides, Carbides, Nitrides, and Silicides, MacMillan Company, New York, 1953.
[2] T.Y. Kosolapova, Carbides: Properties, Production, and Applications, Plenum Press, New York, 1971.
[3] L.E. Toth, Transition Metal Carbides and Nitrides, Academic Press, New York and London, 1971.
[4] O. Hugh, Pierson Handbook of Refractory Carbides and Nitrides, William Andrew Press, New York, 1996.
[5] H.J. Scussel, Friction and Wear of Cemented Carbides, ASM Handbook, vol. 18, ASM International, 1992, p. 795.
[6] R. Dagani, Nanostructured materials promise to advance range of technologies, Chem. Eng. News 23 (1992) 18–24.
[7] S. Ashley, Small-scale structure yields big property payoffs, Mech. Eng. February (1994) 52–57.
[8] L. Leclercq, M. Provost, H. Pastor, G. Grimblot, A.M. Hardy, L. Gengembre, G. Leclercq, Catalytic properties of transition metal carbides. I. Preparation and physical characterizeation of bulk mixed carbides of molybdenum, J. Catal. 117 (1989) 371–383.
[9] L. Leclercq, M. Provost, H. Pastor, G. Grimblot, Catalytic properties of transition metal carbides. II. Activity of bulk mixed carbides of molybdenum and tungsten in hydrocarbon conversion, J. Catal. 117 (1989) 384–395.
[10] R.B. Levy, M. Boudart, Platinum-like behavior of tungsten carbide in surface catalysis, Science 181 (1973) 547–549.

[11] F.H. Ribeiro, R.A. Dalla betta, M. Boudart, J. Baumgartner, E. Iglesia, Reactions of neopentane, methylcyclohexane, and 3,3-dimethylpentane on tungsten carbides: the effect of surface oxygen on reaction pathways, J. Catal. 130 (1991) 86–105.
[12] M.J. Ledoux, C.P. Huu, J. GuillE, R. Dunlop, Compared activities of platinum and high specific surface area Mo_2C and WC catalysts for reforming reactions. I. Catalyst activation and stabilization: reaction of *n*-hexane, J. Catal. 134 (1992) 383–398.
[13] M.K. Neylon, S. Choi, H. Kwon, K.E. Curry, L.T. Thompson, Catalytic properties of early transition metal nitrides and carbideds: *n*-butane hydrogenolysis, dehydrogenation and isomerization, Appl. Catal. A 183 (1999) 253–263.
[14] L.H. Yaverbaum, Technology of Metal Powders Recent Development, Noyes Data Corp., New York, 1980.
[15] L. Gao, B.H. Kear, Synthesis of nanophase WC powder by a displacement reaction process, Nanostruct. Mater. 9 (1997) 205–208.
[16] L. Gao, B.H. Kear, Low temperature carburization of high surface area tungsten powders, Nanostruct. Mater. 5 (1995) 555–569.
[17] B.H. Kear, P.R. Strutt, Chemical processing and applications for nanostructured materials, Nanostruct. Mater. 6 (1995) 227–236.
[18] N.C. Angastiniotis, B.H. Kear, Bulk synthesis of novel nanocrystalline and amorphous tungsten-base materials, Mater. Sci. Forum 179–181 (1995) 357–362.
[19] B.H. Kear, L.E. Mccandlish, Chemical processing and properties of nanostructured WC–Co materials, Nanostruct. Mater. 3 (1993) 19–30.
[20] L.E. Mccandlish, V. Kevorkian, K. Jia, T.E. Fischer, Chemical processing and properties of nanostructured WC–Co materials, Adv. Powder Metall. Part. Mater. 5 (1994) 329–337.
[21] N.C. Angastiniotis, B.H. Kear, L.E. McCandlish, Formation, and alloying of nanostructured b-W powders, Nanostruct. Mater. 1 (1992) 293–302.
[22] L.E. McCandlish, B.H. kear, B.K. Kim, Processing and properties of nanostructured WC–Co, Nanostruct. Mater. 1 (1992) 119–124.
[23] L.E. McCandlish, B.H. Kear, B.K. Kim, Chemical processing of nanophase tungsten carbide–cobalt composite powders, Mater. Sci. Technol. 6 (1990) 953–957.
[24] L.E. McCandlish, R.S. Polizzotti, Control of composition and microstructure in the cobalt–tungsten–carbon system using chemical synthetic techniques, Solid State Ionics 32/33 (1989) 795–801.
[25] M.A. Xueming, J.I. Gang, Structure and properties of bulk nanostructured WC–Co alloy by mechanical alloying, J. Alloys Compd. 264 (1998) 267–270.
[26] G.H. Lee, S. Park, S. Kang, K.H. Chung, E.J. Lavernia, Processing issues for cryomilled WC–Co nanopowders, Mater. Trans. 44 (2003) 1935–1941.
[27] G.M. Wang, P. Millet, A. Calka, S.J. Campbell, Mechanosynthesis of tungsten carbide, Mater. Sci. Forum 179–181 (1995) 183–188.
[28] M.S. El-Eskandarany, A.A. Mahday, H.A. Ahmed, A.H. Amer, Synthesis and characterizations of ball-milled nanocrystalline WC and nanocomposite WC–Co powders and subsequent consolidations, J. Alloys Compd. 312 (2000) 315–325.
[29] Z.Q. Li, H.F. Zhang, X.B. Zhang, Y.Q. Wang, X.J. Wu, Nanocrystalline tungsten carbide encapsulated in carbon shell, Nanostruct. Mater. 10 (1998) 179–184.
[30] B.D. Cullity, Element of X-Ray Diffraction, Addison-Wesley, Reading, MA, 1978.
[31] D.D. Dibitonto, P.T. Eubank, M.A. Barrufet, Theoretical models of the electrical discharge machining process. I. A simple cathode erosion model, J. Appl. Phys. 66 (1989) 4095–4103.
[32] D. Tu, S. Chang, C. Chao, Lin F C., Tungsten carbide phase transformation during the plasma spray process, Vac. Sci. Technol. A3 (1985) 2479–2482.
[33] C. Verdon, A. Karimi, J.-L. Martin, Study of high velocity oxy-fuel thermally sprayed tungsten carbide based coatings. Part 1. Microstructures, Mater. Sci. Eng. A246 (1998) 11–24.
[34] Y. Suda, T. Nakazono, K. Ebihara, K. Baba, R. Hatada, Properties of WC films synthesized by pulsed YAG laser deposition, Mater. Chem. Phys. 54 (1998) 177–180.
[35] S. Sharafat, A. Kobayashi, S. Chen, N.M. Ghoniem, Production of high-density Ni-bonded tungsten carbide coatings using an axially fed DC-plasmatron, Surf. Coat. Technol. 130 (2000) 164–172.
[36] T.B. Massalski (Ed.), Binary Alloy Phase Diagrams, vol. 1: Alloys, vol. 2: Phase Diagrams, ASM International, Materials Park, OH, 1990.
[37] R. Koc, S.K. Kodambaka, Tungsten carbide (WC) synthesis from novel precursors, J. Eur. Ceram. Soc. 20 (2000) 1859–1869.
[38] P.B. Hirsch, Electron Microscopy of Thin Crystals, Krieger Publishing Company, New York, 1977.